

## ON THE LOW FALSE POSITIVE PROBABILITIES OF *KEPLER* PLANET CANDIDATES

TIMOTHY D. MORTON<sup>1</sup>, JOHN ASHER JOHNSON<sup>1,2</sup>  
*Draft version February 4, 2017*

### ABSTRACT

We present a framework to conservatively estimate the probability that any particular planet-like transit signal observed by the *Kepler* mission is in fact a planet, prior to any ground-based follow-up efforts. We use Monte Carlo methods based on stellar population synthesis and Galactic structure models, and we provide empirical analytic fits to our results that may be applied to the as-yet-unconfirmed *Kepler* candidates. We find that the false positive probability for candidates that pass preliminary *Kepler* vetting procedures is generally  $<10\%$  and often  $<5\%$ , assuming a 20% occurrence rate of close-in planets in the mass range  $0.5 M_{\oplus} < M_p < 10 M_{\text{Jup}}$ . This probability varies most strongly with the magnitude and Galactic latitude of the *Kepler* target star, and more weakly with transit depth. We establish that a single deep high-resolution image may be an extremely effective follow-up tool for shallow transit signals. By reducing the radius around the target star where a blend might exist, the false positive probability of an earth-sized transit around a faint star decreases from  $>20\%$  to  $<2\%$ , assuming a continuous power law for the planet mass function with index  $\alpha = -1.5$ . Since *Kepler* will detect many more planetary signals than can be positively confirmed with ground-based follow-up efforts in the near term, these calculations will be crucial to using the ensemble of *Kepler* data to determine population characteristics of planetary systems.

### 1. INTRODUCTION

On the cusp of the first full release of planet candidates from the *Kepler* mission (Koch et al. 1998; Borucki et al. 2008), the study of the properties of exoplanetary systems is entering a new era. For the first time there will exist a large uniform sample of transiting planets unaffected by the detection challenges and selection effects inherent in ground-based searches (Gaudi 2005), enabling a first clear glimpse of the population of exoplanets down to the size of Earth as well as the first opportunity to study planet radii at large orbital separations. However, follow-up observations to unambiguously confirm individual signals are time-consuming and difficult (or impossible), especially for fainter stars and smaller planets. Consequently, in order to understand what the population of *Kepler* transit-like signals can tell us about the population of exoplanets in general, the problem of astrophysical false positives must be understood.

From the early days of planet transit searches, eclipsing binary systems masquerading as transit signals have plagued detection efforts (Konacki et al. 2003; O’Donovan et al. 2006; Poleski et al. 2010; Almenara et al. 2009). Generally speaking, there are three types of astrophysical false positive: a grazing eclipsing binary, a dwarf star eclipsing a giant star, and a blended eclipsing binary system, which may be either a physical triple system or an unassociated binary blended within the aperture of a target star (Torres et al. 2004).

The remarkable photometric precision that *Kepler* is delivering (Jenkins et al. 2010b) allows for an immediate simplification of the false positive landscape. Batalha et al. (2010a) explain the multitude of ways that cer-

tain common false positive scenarios can be identified from *Kepler* photometry alone. For example, grazing eclipsing binaries can be identified by their V-shaped transits, and the giant-eclipsed-by-a-dwarf scenario can be avoided both by the comprehensive work that went into assembling the Kepler Input Catalog (Latham et al. 2005; Batalha et al. 2010b) and by the ability to photometrically identify giants by their elevated levels of stellar variability compared with dwarf stars (Basri et al. 2010). Even many blended binaries can be identified from the *Kepler* photometry and astrometry alone, by looking for a shift in the center of light, e.g the “rain diagrams” of Jenkins et al. (2010a). However, some blended binary scenarios remain undetectable by this technique, especially those in hierarchical triple systems, and so a detailed understanding of the false positive problem for *Kepler* requires a detailed understanding of the probability of encountering such blend scenarios. The *Kepler* team has proven that extremely careful and detailed analysis of individual systems can “validate” planets probabilistically by modeling the light curves of all possible false positive scenarios (Torres et al. 2011), but as this method is extremely computationally intensive, it is impractical to apply to all the candidates.

There has been significant previous effort in the literature dedicated to predicting the expected rate of false positive transit signals. Brown (2003) pioneered this work by predicting the rates of different types of false positives and Jovian planet detections for a variety of different surveys, including the then-future *Kepler* mission. Evans & Sackett (2010) greatly extend this work by deriving detection and false positive rates from full-scale bottom-up simulations of synthetic ground-based transit surveys, taking into account all false positive possibilities and many details not included by Brown (2003). We continue in the tradition of these authors with an analysis directly applicable to the *Kepler* mission, approaching from a slightly different angle. Instead of focusing on

tdm@astro.caltech.edu  
johnjohn@astro.caltech.edu

<sup>1</sup> Department of Astrophysics, California Institute of Technology, MC 249-17, Pasadena, CA 91125

<sup>2</sup> NASA Exoplanet Science Institute (NExScI)

predicting an overall number or expected rate of planet detections or false positives, we instead seek a simple answer to the following question: “What is a conservative estimate of the probability that an observed apparent transit signal is in fact a true transiting planet?” By framing the issue in this manner we are able to sidestep the complex issue of detectability, as our analysis assumes a detected transit candidate.

Our philosophy in this work is not to take into account all conceivable details of transit signals, but rather to consider only those which are most salient: the brightness of the *Kepler* target star, its location in the field, and transit signal depth. The details we choose not to address in this work (notably transit period and duration) are those we judge would add uncertainty to our calculations while tending to only decrease our estimates of the false positive probability. Thus we are able to keep our analysis straightforward, yet remain confident we are calculating conservative upper limits to the probability that any given *Kepler* transit signal might be a false positive. As we show in §2 and again in §3, even these conservative upper limits are enough to indicate that *Kepler* planet candidates will only rarely turn out to be false positives.

## 2. BASIC BAYESIAN FRAMEWORK

The probability that a given transit signal is of planetary origin may be expressed as the following, according to Bayes’ theorem:

$$\Pr(\text{planet} \mid \text{signal}) = \frac{\Pr(\text{signal} \mid \text{planet})\Pr(\text{planet})}{\Pr(\text{signal})}. \quad (1)$$

In this framework  $\Pr(\text{signal} \mid \text{planet})$  is the probability of obtaining the observed signal given that there is a transiting planet on an orbit of a particular period. This factor is known as the *likelihood* of the signal under the planet hypothesis, and we will abbreviate it as  $\mathcal{L}_{\text{pl}}$ .  $\Pr(\text{planet})$  is the probability of a star hosting a transiting planet (the occurrence rate of planets times the transit probability), which must enter the calculation as an *a priori* assumption. Thus we call this factor, according to Bayesian convention, the *prior* on planets, and designate it  $\pi_{\text{pl}}$ .

Since there are only two possible origins of a transit-like signal (planet or false positive), the denominator of Equation 1 can be rewritten as marginalizing over the possible models:

$$\Pr(\text{signal}) = \mathcal{L}_{\text{pl}}\pi_{\text{pl}} + \mathcal{L}_{\text{FP}}\pi_{\text{FP}}. \quad (2)$$

Using our convention,  $\mathcal{L}_{\text{FP}}$  and  $\pi_{\text{FP}}$  are the likelihoods and priors for a false positive signal. The false positive term can be further broken down accounting for the two specific false positive scenarios we are exploring: the blended eclipsing binary (BB) and the physical eclipsing triple (PT), allowing Equation 1 to be rewritten as the following:

$$\Pr(\text{planet} \mid \text{signal}) = \frac{\mathcal{L}_{\text{pl}}\pi_{\text{pl}}}{\mathcal{L}_{\text{pl}}\pi_{\text{pl}} + \mathcal{L}_{\text{BB}}\pi_{\text{BB}} + \mathcal{L}_{\text{PT}}\pi_{\text{PT}}}. \quad (3)$$

In general, the likelihoods depend on the particularities of the transit signal and enable discrimination between models depending on the transit depth, shape, or period.

For now we ignore these details, assuming for the moment that we have no knowledge of the differences between the kind of transit signals to expect from planets and from false positives. This enables us to write a simplified version of Eq. 3:

$$\Pr(\text{planet} \mid \text{signal}) \approx \frac{\pi_{\text{pl}}}{\pi_{\text{pl}} + \pi_{\text{BB}} + \pi_{\text{PT}}}. \quad (4)$$

We then define the “false positive probability” (FPP) as the complement of this probability:

$$\text{FPP} = 1 - \Pr(\text{planet} \mid \text{signal}) \quad (5)$$

Thus, before considering any detailed information of a particular light curve, the probability that an observed transit signal is actually a false positive depends only on the relative occurrence rates of planets and the false positive scenarios. As mentioned above,  $\pi_{\text{pl}}$  is simply an assumed occurrence rate of planets times the transit probability; we explain how we determine  $\pi_{\text{BB}}$  and  $\pi_{\text{PT}}$  in the following subsections. We explain first this priors-only framework in order to elucidate what dominates our final results, but in §3 we will include the likelihoods we removed in Equation 4, taking into account dependence on the depth of the transit signal.

### 2.1. Blended Binaries

The probability of a transit-mimicking binary system to be blended within the PSF of a *Kepler* target star ( $\pi_{\text{BB}}$ ) can be broken down into the following way:

$$\pi_{\text{BB}} = \Pr(\text{blend}) \cdot \Pr(\text{appropriate eclipsing binary}). \quad (6)$$

The first factor here is the probability for a potentially blending star to be projected within a given radius of a *Kepler* star, and the second is the probability for that star to be an eclipsing binary system that can appropriately mimic a planetary transit.

To calculate these probabilities, we use the stellar population synthesis and Galactic structure code TRILEGAL (TRIdimensional modeL of thE GALaxy; Girardi et al. (2005)), which is publicly available on the web<sup>3</sup>. TRILEGAL simulates the physical and photometric properties of the stars along a given line of sight, using various stellar evolution grids (Girardi et al. 2002; Chabrier et al. 2000) and a Galactic model that includes a halo, thin and thick disks, and a bulge. All of our simulations use a Chabrier lognormal IMF (Chabrier 2001) and default TRILEGAL values for the Galactic structure parameters, including a squared hyperbolic secant structure for the thin disk, an exponential structure for the thick disk, and an oblate spheroid for the halo.

#### 2.1.1. Probability of a blend

The blend probability can be calculated by determining the average sky density (e.g. stars per square arcsec) of stars faint enough so as not to be obviously present yet bright enough to possibly mimic a transit. The first condition is somewhat subjective, and we conservatively say that a star must be more than 1 magnitude fainter than the *Kepler* primary in order to be able to hide undetected within the *Kepler* aperture. In practice the true value

<sup>3</sup> <http://stev.oapd.inaf.it/cgi-bin/trilegal>

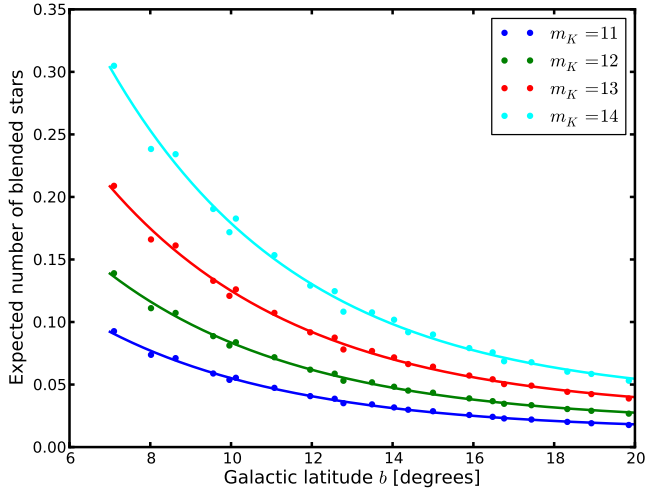


FIG. 1.— The probability for a possibly blending star to be projected within  $2''$  of a *Kepler* target star, as a function of Galactic latitude, as determined by TRILEGAL simulations. The plotted points are simulations; the lines are the exponential fits as described in Equation 8.

is probably significantly fainter, but this approximation will lead to only a small overestimate of the blended star probability, as there are many more faint than bright stars.

The faint condition can be determined by noting that in order for a blended eclipsing binary system to mimic a transit of fractional depth  $\delta$ , the blended system must comprise more than a fraction  $\delta$  of the total flux within the *Kepler* aperture. This condition may be expressed as the following:

$$m_{K,\text{bin}} - m_{K,\text{target}} = \Delta m_K = -2.5 \log_{10}(\delta), \quad (7)$$

where  $m_{K,\text{bin}}$  is the total apparent *Kepler* magnitude of the blended binary system and  $m_{K,\text{target}}$  is the magnitude of the *Kepler* target star. A transit depth of  $\delta = 0.01$  corresponds to  $\Delta m_K = 5$ ; for  $\delta = 10^{-3}$ ,  $\Delta m_K = 7.25$ ; and for  $\delta = 10^{-4}$  (approximately an Earth-sized transit of a Solar-radius star),  $\Delta m_K = 10$ . This means that no binary system fainter than  $m_K = 24$  can possibly mimic a  $\delta = 10^{-4}$  transit around a  $m_K = 14$  star, which is a typical magnitude for a *Kepler* target.

Using TRILEGAL, we determine the sky density of stars in this magnitude range within the *Kepler* field, and thus the probability of one by chance being projected close to a *Kepler* target star, by simulating a  $10 \text{ deg}^2$  field centered on the center of the *Kepler* field. We then simply count the stars within the desired range of *Kepler* magnitude (which TRILEGAL provides). As a fiducial example, the average density of stars between  $m_K = 15$  and  $m_K = 23.25$ , the range corresponding to a  $\delta = 10^{-4}$  transit of a  $m_K = 14$  star, is  $0.0085 \text{ stars-arcsec}^{-2}$ . The probability of any given small circle on the sky containing one of these stars is then simply the area of the circle multiplied by this density. Continuing this example, ( $m_K = 14, \delta = 10^{-4}$ ) the probability of such a star being within  $2''$  of a *Kepler* target star is 0.11.

However, because the *Kepler* field is quite extended and centered only a few degrees off the Galactic plane, there is a considerable gradient in background stellar

TABLE 1  
POLYNOMIAL COEFFICIENTS<sup>1</sup> FOR EQUATION 14

	$c_0$	$c_1$	$c_2$	$c_3$	$c_4$
A	-75.9827	24.33862	-2.89554	0.15122	-2.8898e-3
B	106.6416	-33.0161	3.95499	-0.20745	4.0288e-3
C	-8.2032e-2	3.3856e-2	-5.4119e-3	3.3678e-4	-7.0361e-6
D	5.7077e-3	-1.3166e-3	9.9054e-5	-2.4401e-6	—
E	-0.11737	2.8425e-2	-2.2086e-3	5.5916e-5	—

<sup>1</sup> This table lists the polynomial coefficients for the empirical fits to how the blended binary false positive probability as a function of Galactic latitude changes with *Kepler* magnitude  $m_K$ . A, B, C, D, and E are functions of  $m_K$ , valid between  $m_K = 11$  and  $m_K = 15$ . The polynomials are of the form  $c_0 + c_1 A + c_2 A^2 + c_3 A^3 + c_4 A^4$ .

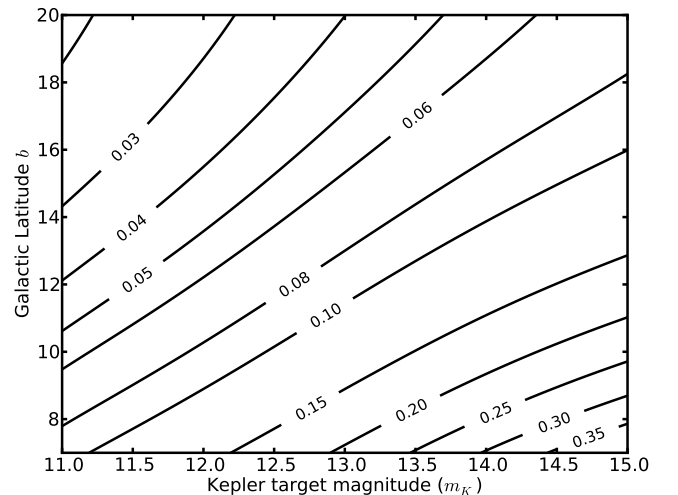


FIG. 2.— The probability for a possibly blending star to be projected within  $2''$  of a *Kepler* target star, as a function of both Galactic latitude, and target star magnitude, as determined by TRILEGAL simulations.

density across the field that must be accounted for. To accomplish this, we simulate 21 different  $5 \text{ deg}^2$  fields, each centered on one of the *Kepler* double-CCD squares. The resulting probabilities are plotted in Figure 1 as a function of Galactic latitude, for the magnitude ranges corresponding to  $m_K = 11, 12, 13, 14$ , and 15. Recognizing that this blend probability appears to be exponentially related to Galactic latitude  $b$ , and that the nature of the exponential depends on  $m_K$ , we fit an analytic expression of the following form:

$$p_{\text{blend}}(b, m_K) = C(m_K) + A(m_K)e^{-b/B(m_K)}, \quad (8)$$

where  $A$ ,  $B$ , and  $C$  are all polynomial functions of *Kepler* magnitude, with the coefficients listed in Table 1. These fits are valid between  $m_K$  values of 11 and 15, and  $b$  values between  $7^\circ$  and  $20^\circ$  (the approximate extent of the *Kepler* field). Figure 2 graphically illustrates the behavior of Equation 8.

### 2.1.2. Probability of an appropriate eclipsing binary

The probability that a blended star is an appropriately configured eclipsing binary system depends first on the binary fraction of blending stars, and secondly on both the distribution of binary properties and the magnitude of the *Kepler* target star. Of central importance is that

TABLE 2  
PREDICTED FALSE POSITIVE PROBABILITIES: BASIC FRAMEWORK

Experiment (1)	Threshold (2)	Blend Radius (3)	< # blends > (4)	$\pi_{\text{BB}}$ (5)	$\pi_{\text{PT}}$ (6)	$\pi_{\text{pl}}$ (7)	FPP (8)
<i>Kepler</i>	$10^{-4}$	2''	0.11	$1.1 \times 10^{-4}$	$1.2 \times 10^{-4}$	0.01	<b>0.02</b>
Wide-Field Survey (e.g. HATNet)	0.005	14''	1.67	0.0014	$2.7 \times 10^{-4}$	$5 \times 10^{-4}$	<b>0.77</b>
CoRoT	$10^{-3}$	10''	2.71	0.0035	$1.4 \times 10^{-4}$	0.01	<b>0.27</b>

(1) Name of a transit survey

(2) Fractional depth detection threshold

(3) Effective aperture size inside which a blended star might reside. *Kepler* can restrict this radius to 2'' by centroid analysis.

(4) The expected number of blending stars expected per aperture, based on estimates of the density of stars within the possibly-blending magnitude range for each experiment.

(5) The rate we calculate for the blended eclipsing binary false positive scenario

(6) The rate we calculate for the physical eclipsing triple false positive scenario

(7) The assumed rate of detectable transiting planets

(8) False positive probability =  $\pi_{\text{pl}}/(\pi_{\text{BB}} + \pi_{\text{PT}} + \pi_{\text{pl}})$

in order for a blended binary to successfully mimic a *Kepler* planet transit candidate, it must both have a diluted primary eclipse shallow enough to look like a planet and a diluted secondary eclipse shallow enough so as not to be detected.

The apparent fractional “transit” depth of a blended binary system depends on the intrinsic binary system eclipse depth  $\delta_b$ , and the relative apparent magnitudes of the *Kepler* target star and the blended system:

$$\delta = \delta_b \cdot 10^{-0.4(m_{K,\text{bin}} - m_{K,\text{target}})}. \quad (9)$$

The primary and secondary eclipse depths of the binary system are the following:

$$\delta_{b,\text{pri}} = \frac{\left(\frac{R_2}{R_1}\right)^2 F_1}{F_1 + F_2}, \quad (10)$$

and

$$\delta_{b,\text{sec}} = \frac{F_2}{F_1 + F_2}, \quad (11)$$

where  $R_1$  and  $F_1$  are the stellar radius and flux in the *Kepler* band of the larger of the two stars, and  $R_2$  and  $F_2$  are of the smaller star.

The conditions we define for a binary to be “appropriate” are for the diluted primary eclipse depth to be between 0.02 and  $10^{-4}$  (shallow enough to look like a planet, but still detectable), and for the diluted secondary to be shallower than  $10^{-4}$  (undetected). We recognize that “detectability” of a transit is a function of more than just the transit depth, but for our purposes we use a depth of  $10^{-4}$  as the detection threshold. A more detailed population study based on *Kepler* candidates should use rather the signal-to-noise ratio of a transit as the criterion for detectability (Beatty & Gaudi 2008). However, as our framework deals with how to interpret signals once they are detected, careful detectability analysis is unnecessary.

To calculate the probability of all these conditions being met (a star being binary and being “appropriate”), we use the TRILEGAL simulations and assume binary properties according to the work of Raghavan et al. (2010). That is, we assume a flat mass ratio distribution between 0.1 and 1 (Raghavan et al. (2010) actually

observes the distribution to be flat between about 0.2 and 1, but we extend it to 0.1 to be more conservative).

For each star in a particular TRILEGAL line-of-sight simulation that lies in the appropriate magnitude range (§2.1.1), we first randomly assign it to be a binary or not and then calculate what the primary and secondary diluted depths would be if the system were eclipsing and blended with a *Kepler* target star of a particular magnitude.  $R_1$  and  $F_1$  are provided by TRILEGAL<sup>4</sup>, and we determine  $R_2$  and  $F_2$  based on a randomly assigned mass ratio and the Padova models at the age of the primary. Given these system parameters, we can then randomly determine if each system undergoes a non-grazing eclipse, according to the probability that each system will be in such an orientation:

$$\text{Pr}(\text{eclipse}) = \frac{R_1 - R_2}{a}, \quad (12)$$

where  $a$  is the orbital semi-major axis, determined from Kepler’s law.

From this procedure, using a *Kepler* target star of  $m_K = 14$ , an orbital period of 10 days, and a line-of-sight simulation at the center of the *Kepler* field, we find that 1.25% of binaries have non-grazing eclipses and about 20% of those eclipsing binaries are “appropriate.” Combined with a  $\sim 40\%$  binary fraction<sup>5</sup>, this results in a probability of 0.001 for a star to be an appropriate eclipsing binary, giving a value of  $\pi_{\text{BB}} = 0.11 \times 0.001 = 1.1 \times 10^{-4}$  for the center of the *Kepler* field.

As in §2.1.1, we empirically investigate how this probability changes as a function of galactic latitude and target star magnitude. We find the behavior for any particular magnitude is well described by a shallow linear relation in  $b$ :

$$\text{Pr}(\text{appropriate ecl. binary}) = bD(m_K) + E(m_K), \quad (13)$$

where again the variation of the values of the coefficients

<sup>4</sup> This properly accounts for the possibility that the blend might be an evolved system; e.g. a dwarf star eclipsing a giant.

<sup>5</sup> To be precise, we actually use a binary fraction function that increases with stellar mass: 40% for  $M < M_\odot$ , 50% for  $M_\odot < M < 1.5M_\odot$ , and 75% for  $M > 1.5M_\odot$ , roughly adapted from Figure 12 in Raghavan et al. (2010). This is a conservative estimate of the binary fraction, as the Raghavan Figure includes multiple systems as well as binaries.

$D$  and  $E$  is modeled well with a polynomial in  $m_K$  (Table 1).

Multiplying Equation 13 with Equation 8 then gives a full analytic expression for the probability of a star of given Kepler magnitude at a given Galactic latitude to be blended with an eclipsing binary system able to mimic a planetary transit:

$$\pi_{\text{BB}}(m_K, b) = [C(m_K) + A(m_K)e^{-b/B(m_K)}] \times [bD(m_K) + E(m_K)], \quad (14)$$

where  $A, B, C, D$ , and  $E$  are polynomial functions of  $m_K$  with coefficients given in Table 1.

### 2.2. Physical Triples

The probability that a *Kepler* target star is in fact a physical triple system configured such that it might be able to mimic a planetary transit ( $\pi_{\text{PT}}$ ) can be broken down as follows:

$$\pi_{\text{PT}} = \text{Pr}(\text{triple}) \cdot \text{Pr}(\text{eclipsing and appropriate}). \quad (15)$$

The first factor is simply the frequency of triple systems, which Raghavan et al. (2010) determine to be 8% for sun-like stars. The fraction of triple systems that are of appropriate configuration can be determined by using the same conditions as we used above in §2.1.2. That is, we require the diluted eclipse depths (Eqs. 9-11) to be between  $0.02$  and  $10^{-4}$ , except this time one of the three triple components provides the diluting flux.

We assume two different hierarchical possibilities for triple systems. Referring to the three components in order of descending mass as A, B, and C, the triple system may either be set up as A + BC, where B & C are the closer potentially eclipsing pair and A is the diluting star, or as AC + B, with A & C as the closer pair and B diluting. We ignore the case AB + C because the faintest component being the diluting star would be unable to mimic a planet transit.

We calculate the probability that a triple system will be eclipsing and “appropriate” (again assuming a 10-day orbit) as follows:

$$p_a = \int \int A(M_A, q_1, q_2) \Phi_q dq_1 \Phi_q dq_2. \quad (16)$$

$A(M_A, q_1, q_2)$  equals 1 if the system is eclipsing and can mimic a transit and 0 if not, and the mass ratios  $q_1 \equiv M_B/M_A$  and  $q_2$  (either  $M_C/M_A$  or  $M_C/M_B$ , with 50/50 odds) determine the architecture of the triple system.  $\Phi_q$  is the mass ratio distribution that we used in §2.1.2 (flat between 0.1 and 1). We assign the radius and flux of each component according to the Padova model grids in order to calculate both the non-grazing eclipse probability and the diluted eclipse depths. Evaluating this integral numerically we obtain  $p_a = 0.0015$ , which results in  $\pi_{\text{PT}} = 0.08 \times 0.0015 = 1.2 \times 10^{-4}$ .

Unlike the blended eclipsing binary scenario, the probability of a target being a physical eclipsing triple does not depend either on galactic latitude or apparent magnitude. There is a very weak dependence on stellar mass of the primary, but for our calculations we just assume that all target stars have masses close to  $1 M_\odot$ , which is reasonable as *Kepler* is specifically targeting solar-type stars.

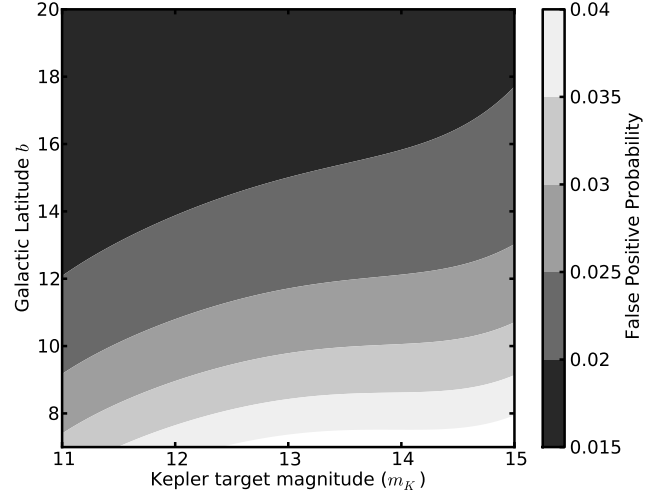


FIG. 3.— The false positive probability of a *Kepler* candidate, according to our basic framework (i.e. independent of  $\delta$ ), as a function of target star magnitude  $m_K$  and galactic latitude. A planet occurrence rate of 20% is assumed. This plot assumes that *Kepler* is able to internally restrict the radius inside which a possible blended binary might reside to  $2''$ .

### 2.3. Basic Framework: Summary and Discussion

Now that we have determined the priors for both false positive scenarios, we are able to evaluate the FPP (Equations 4 and 5) by assuming a frequency of close-in planets. We adopt a 20% frequency according to the results of the *NASA-UC Eta-Earth Survey* of Howard et al. (2010). This conservative estimate of 20%, combined with a 5% transit probability for a planet on a 10-day orbit (the period we have been assuming up to now) gives  $\pi_{\text{pl}} = 0.01$ . From a planet detection standpoint, this result is promising, as it gives a 98% probability that an observed planet-like transit signal around a  $m_K = 14$  star in the middle of the *Kepler* field is authentic, and thus an FPP of only 2%. Because of the variation of the background stellar density across the field, this value varies with Galactic latitude and  $m_K$ , as shown in Figure 3. This is a remarkable result, as it indicates that almost every signal that passes the *Kepler* astrometric and photometric false positive tests is likely a planet transit, before any RV confirmation attempts.

One might rightly pause at this juncture and wonder how the false positive probability for *Kepler* can be so low. After all transit searches up until now, both ground-based (e.g. HAT, WASP) and space-based (e.g. CoRoT) been plagued by false positives (Konacki et al. 2003; O’Donovan et al. 2006; Poleski et al. 2010; Almenara et al. 2009). To address this, consider what Equation 4 would say about the probability of a transit signal being true for those experiments; these results are summarized in Table 2.

Taking the Hungarian-made Automated Telescope Network (HATNet) as an example of a ground-based survey, we note that its 11cm telescopes produce a photometric aperture of about  $14''$  in radius (Hartman et al. 2004). Using this radius and a depth of 0.5% as a detection threshold, we repeat the analysis of §2.1, using the line-of-sight simulation at the center of the *Kepler* field

for the sake of comparison. For the probability of a possibly blending star to be within the aperture we obtain 1.67, which must obviously now be interpreted as an average number of blending stars per aperture instead of a probability. For the probability of a blending star to be an appropriate eclipsing binary we obtain  $8.4 \times 10^{-4}$ , giving  $\pi_{\text{BB}} = 1.67 \times 8.4 \times 10^{-4} = 0.0014$ . Following §2.2 we calculate  $\pi_{\text{PT}} = 2.7 \times 10^{-4}$ . Finally, taking into account that the probability of a sun-like star hosting a planet easily detectable by this survey is only about 1%<sup>6</sup>, then  $\pi_{\text{pl}} = 0.01 \times 0.05 = 5 \times 10^{-4}$  for this survey. This results in an FPP of 0.77 for a hot Jupiter-like transit signal for a HAT-like ground-based search, according well with Latham et al. (2009), who describe the results of follow-up efforts of a sample of transit candidates, eight of which turned out to be blended binaries and one to be a planet.

The space-based mission CoRoT (Baglin 2003) has also had difficulties with false positives. Though it obtains much better photometric precision than a ground-based search and benefits from uninterrupted observing, its large, 320 arcsec<sup>2</sup> aperture (Almenara et al. 2009) results in an expected number of 2.71 blended stars for a  $m_K = 14$  target star. In addition, its photometric precision is about one part in  $10^3$ , resulting in  $\pi_{\text{BB}} = 0.0035$ , and  $\pi_{\text{PT}} = 1.4 \times 10^{-4}$ . Assuming then a 20% occurrence rate of planets detectable by CoRoT, this gives an FPP of 0.27. At first this appears to somewhat contradict Almenara et al. (2009), who reported 6 planets and 25 diluted binaries among CoRoT’s “solved candidates” (ignoring the “undiluted binary” category, as we are not considering that possibility for *Kepler*). However, if one considers how much easier (and faster) it is to identify a false positive than to positively confirm a planet, this prediction can certainly be consistent with these results, as only 49 of their 122 candidates had been solved at the time.

Another reasonable question to ask is how uncertainties in our models and assumptions propagate through to uncertainties in FPP. This is challenging to address exactly, as our analysis rests on the results from TRI-LEGAL simulations, stellar model grids, and various assumptions about multiple star systems. Rather than attempt a detailed start-to-finish treatment of all the uncertainties, we instead investigate what happens if we artificially inject fractional uncertainties into our prior calculations and simulate the results according to our analytic fits. We find that 20% fractional uncertainties in background stellar density, appropriate eclipse probability, and physical eclipsing triple probability lead to 17% fractional uncertainty in FPP. This is a fiducial example, and the uncertainty in FPP scales linearly with these component uncertainties.

One might also wonder how sensitive our derived FPP for *Kepler* is to the assumption that 20% of stars host planets, as well as how justifiable such an assumption may be. We address these questions in Figure 4. A 20% occurrence rate lies in the middle of the measured occurrence rate of planets with minimum masses  $> 3M_{\oplus}$  and periods  $< 50$  days from the *NASA-UC Eta-Earth Survey* of Howard et al. (2010). In addition, even the most pessimistic interpretation of the results from  $\eta_{\text{earth}}$

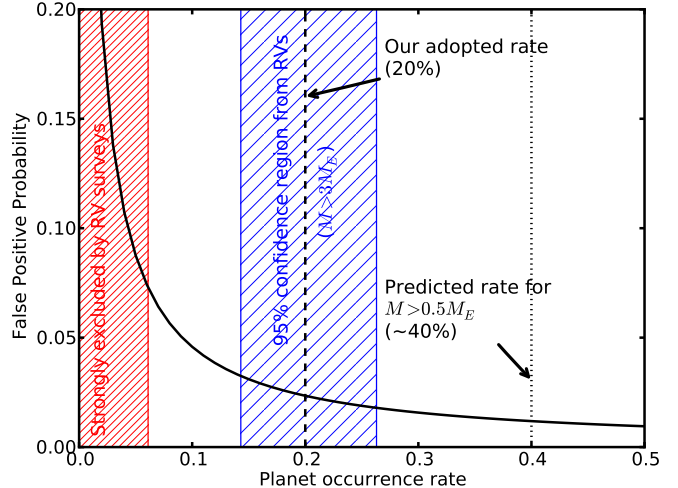


FIG. 4.— False positive probability as a function of assumed planet occurrence rate, for a  $m_K = 14$  target star in the center of the *Kepler* field. The occurrence rate of planets detectable by *Kepler* is not known for sure, but RV surveys, especially the *NASA-UC Eta-Earth Survey* of Howard et al. (2010), have made inroads in measuring the fraction of stars hosting low-mass planets. The hashed area below 9% represents the occurrence rate of planets with  $P < 50$  days that is ruled out with 95% confidence by  $\eta_{\text{earth}}$ , counting only the firm detections, and not correcting for completeness. The central hashed area represents the 95% confidence region calculated including candidate planets and completeness correction, for minimum masses greater than  $3M_{\oplus}$ . Extrapolating their observed mass distribution down to  $0.5M_{\oplus}$  brings their total estimated planet occurrence rate to 43%. Overall, this plot shows that our derived FPP cannot reasonably be any higher than 7% if our planet occurrence estimate is incorrect, and will likely be lower.

allows for a minimum of a 9% occurrence rate, which would still imply an FPP of only 7%. More likely, the true occurrence rate is somewhat higher than our assumption, if not as high as the  $\sim 40\%$  implied by a naïve extrapolation of the observed power law-like distribution down to  $0.5M_{\oplus}$ . We note that the *NASA-UC Eta-Earth Survey*, as with all RV surveys, is only able to measure minimum masses and thus that the interpretation of the true mass of any individual detection is dependent on an assumption of the overall form of the planet mass function (Ho & Turner 2010). However, when an ensemble of minimum mass measurements is available and its distribution resembles a power law with index  $\alpha < -1$ , the most likely explanation is that the true mass function follows a similar power-law shape.

In summary we may say that several factors contribute to *Kepler* being able to minimize the false positive problem compared to previous transit surveys. First, its ability to astrometrically rule out wide blend scenarios helps mitigate the issue of blended binaries. Secondly, its photometric precision enables it to identify many false positives based on their secondary eclipses. And lastly, *Kepler* is sensitive to lower-mass planets, which are significantly more common than the larger planets to which ground-based surveys are sensitive.

### 3. DETAILED FRAMEWORK: CONSIDERING TRANSIT DEPTH

We note that we have not yet discussed any details of the transit signal besides its existence, though some of

<sup>6</sup> for  $P < 11.5\text{d}$  and  $M > 0.5M_J$ ; Cumming et al. (2008)

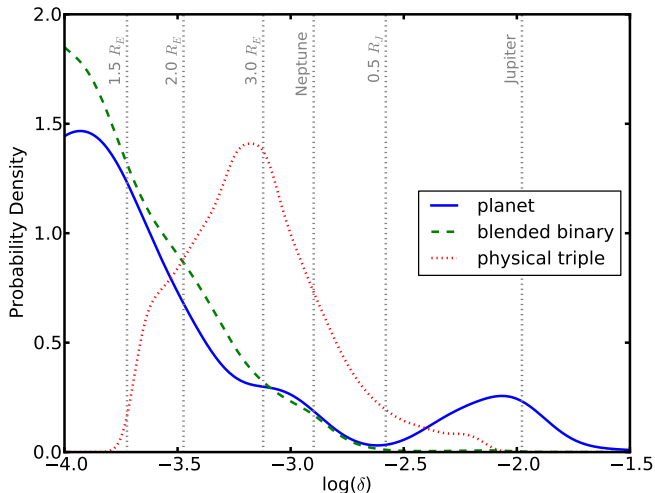


FIG. 5.— Distributions of apparent “transit” depths  $\delta$  for different scenarios. The planet distribution comes from an assumed continuous power law in mass, with radii calculated according to models of Fortney et al. (2007) and Seager et al. (2007)

these details may be important. For example, one might expect positive blended binaries to be more common at shallower depths (since faint stars are more common than bright stars, and thus more likely to be blended), which might make the BB scenario more of a problem for earth-sized transit signals. We have also assumed that planets and eclipsing binaries have the same eclipse probability (allowing us to cancel the likelihood factors in Equation 3), though this is not exactly true either, as both the orbital separations of the systems and the radii of the objects are different. And finally, for fainter stars and shallower eclipses, it may be more difficult for internal *Kepler* procedures to astrometrically identify blends.

With these concerns in mind, we may pursue a more detailed analysis of any particular transit. There are many features of transit light curves that might all be used in this exercise, but for now we only take into account the depth of the signal, as that is the most easily measured and easily understood quantity. In this case, Equation 3 becomes:

$$\Pr(\text{pl}|\delta) = \frac{\mathcal{L}_{\text{pl}}(\delta)\pi_{\text{pl}}}{\mathcal{L}_{\text{pl}}(\delta)\pi_{\text{pl}} + \mathcal{L}_{\text{BB}}(\delta)\pi_{\text{BB}} + \mathcal{L}_{\text{PT}}(\delta)\pi_{\text{PT}}}. \quad (17)$$

Here the likelihood functions provide a means to quantify the extent to which the conclusions of our simple framework may change as a function of transit depth  $\delta$ .

Figure 5 shows the likelihoods that we estimate for the three different scenarios as a function of depth. The distribution of depths for the blended binary and physical triple scenarios are determined from the same calculations that we used to compute the priors, except rather than just counting all the systems that give depths that are both planetary and detectable, we keep track of the depth of each simulated false positive and build up  $\delta$  distributions. We find the  $\delta$  distribution for planets by assuming just a simple continuous power law distribution of masses ( $dN/dM \propto M^{-1.5}$ )<sup>7</sup> and converting mass

<sup>7</sup> similar to Howard et al. (2010); Tabachnik & Tremaine (2002)

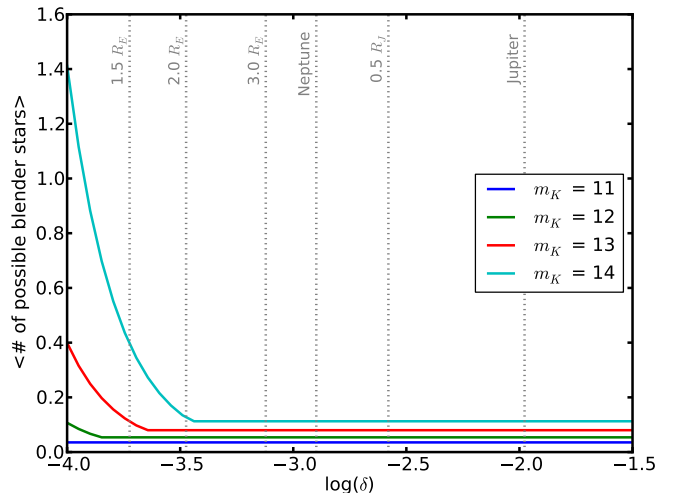


FIG. 6.— As stars get fainter and transit signals get shallower, the ability for *Kepler* to observe a centroid shift indicative of a displaced blended eclipsing binary decreases. We parametrize this effect according to Equation 18.

to radius using the models of Fortney et al. (2007) for giant planets and Seager et al. (2007) for masses below the range of the Fortney models. We then convert the radius distribution into a  $\delta$  distribution assuming a star of  $R = R_{\odot}$ , statistically including the effect that there might be a blending star in the aperture slightly diluting the eclipse depth.

Both of the planetary mass-radius relations we use require assumptions: for the Seager models we assume compositions of solid planets evenly distributed in a 1:1:1 ratio between iron, rock, ice, and a mixture of all three; and for the Fortney models we assume a 1:1:1 distribution between 10, 25, 50, and 100  $M_E$  core masses. We note the “valley” in the radius distribution of planets around  $0.5 R_J$ ; neither solid nor giant planet models can easily produce planets of such radius, as it would require either an extremely large solid planet or an extremely core-heavy gas giant. Thus, a prediction of our assumed mass/radius distribution is that planets of this size should be rare.

Another factor that should vary as a function of  $\delta$  is the ability of *Kepler* to astrometrically identify displaced blends. In §2 we assumed a radius of  $2''$  inside which a blend might reside. However, this radius should increase as transits get shallower and stars get fainter and the signal-to-noise of the centroid shift signal decreases. This is a question that the *Kepler* team should be able to address using simulations of its offset-detecting procedures, but for our purposes we use the radius that the *Kepler* team obtained for Kepler 10-b ( $1''.17$ )<sup>8</sup> and assume scaling with  $\delta$  and  $m_K$  as follows:

$$r = 1.17'' \sqrt{10^{-0.4(11-m_K)}} \left( \frac{\delta}{1.5 \times 10^{-4}} \right)^{-1}, \quad (18)$$

with 11 being the  $m_K$  value for Kepler 10. To be conservative we set the minimum  $r$  to be  $2''$  if this expression gives a smaller value. On the high end, we cap the radius

<sup>8</sup> Batalha et al. (2011), online draft

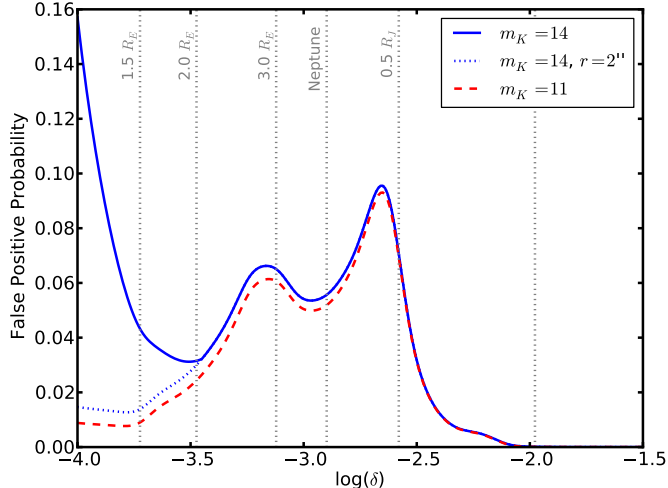


FIG. 7.— The probability that a signal of a given depth will be a false positive, shown for both an  $m_K = 11$  and an  $m_K = 14$  star and assuming a stellar radius of  $R_\odot$  and a Galactic latitude in the center of the *Kepler* field. A planet occurrence rate of 20% is assumed. Note that the false positive probability peaks around depths corresponding to slightly larger than the radius of Neptune, due to the relative dearth of predicted planets of that size and the peak there in the physical triple  $\delta$  distribution. For the fainter star, the false positive probability increases for shallower transits because it becomes more difficult for *Kepler* to rule out displaced blended binaries via astrometry. However, if a single high-resolution image is able to restrict the blend radius to  $2''$ , then the FPP for small  $\delta$  signals is drastically reduced.

at  $10''$ . This is likely an overestimate of the maximum possible blend radius, the exact value of which depends on how many pixels are used in the *Kepler* photometry. The square root factor accounts for a diminishing number of photons received as the target star gets fainter, and the inverse relationship with delta is because the centroid shift scales as  $\delta: \Delta C \sim \delta \cdot r$ . Figure 6 illustrates this effect; bright stars and deeper transits give  $\text{Pr}(\text{blend}) = 0.11$ , as determined in §2.1.1, but as the target star gets fainter and the signal shallower, the expected number of possibly blending stars begins to increase substantially.

#### 4. RESULTS, DISCUSSION AND CONCLUSIONS

The adoption of these more detailed considerations enables us to estimate the FPP as a function of  $\delta$  for a star of given apparent Kepler magnitude (Figure 7). We first note that over the whole range of  $\delta$ , the FPP generally remains below 10%, indicating that these additional considerations do not significantly change the qualitative conclusions we reached within the simple framework. The majority of transit signals in the *Kepler* data release will be actual planets.

We next draw attention to several features of the plot. First, we notice that any approximately Jupiter-sized candidate, whether around a bright star or faint, is almost certainly a planet. This is simply because it is extremely difficult to arrange a diluted binary system with a Jupiter-sized primary depth and an undetectable secondary eclipse.

The second features of interest are the peak in FPP around  $\log \delta = -2.7$  and plateau down to  $\sim 3 R_\oplus$ . The

origin of the peak may be understood by examining Figure 5 and recalling that the mass-radius relation models we use predict a dearth of planets around half of Jupiter’s radius. The plateau corresponds to the range of  $\delta$  which we predict physical triple false positives to populate. Together, these effects conspire to raise the priors-only estimated FPP from §2.3 by a factor of 5 or so.

The third significant feature is the rise in FPP towards shallow depths for a target star of Kepler magnitude  $m_K = 14$ , and the absence of such a rise for the brighter  $m_K = 11$  star. This is caused by the effect illustrated in Figure 6, where the radius outside of which blends may be ruled out by *Kepler* astrometry should increase with smaller eclipse depth and fainter stars. Figure 7 also illustrates the power of a single deep high-resolution image of any low-amplitude candidate system: any progress in shrinking the radius inside which a blended binary may reside will significantly decrease the FPP for Earth-sized transit signals, under the assumption that the occurrence rate of planets rises toward smaller masses.

We note that the plots in Figure 5 are only for particular chosen values of magnitude and a single Galactic latitude in the middle of the *Kepler* field. We present a more comprehensive illustration of the FPP manifold in Figure 8, choosing three specific values of  $\delta$  to illustrate how the FPPs for different types of signals vary with target star magnitude and Galactic latitude. Earth-sized transits have a much steeper gradient across the field and towards fainter stars; this is a result of increasing contribution to the FPP from blended binaries in this region (see Figure 2), combined with the increased blend radius for a shallow transit (Figure 6). On the other hand, Neptune-sized transits have an overall higher FPP than the smaller signal, but with less variation with magnitude and latitude; this is because the FPP for Neptunes is dominated by physical triples. Jovian-sized planets have low FPPs no matter where they occur.

The precise behavior of the FPP distributions of course depends on the input assumptions about the planet population we have used. There are indications from both simulations (Mordasini et al. 2009; Ida & Lin 2004) and simple formation considerations that the mass distribution of planets should not be expected to be a continuous power law. However, RV surveys do seem to indicate a planet mass function that rises towards smaller planet mass (Howard et al. 2010), which appears consistent with a power law. The distribution might turn over below the detectability limit of the Howard et al. survey; which would change the shape of the  $\delta$  distribution in Figure 5 and thus increase the FPP towards smaller depths. There are also uncertainties in the theoretical planet mass-radius relationships, which depend most directly on the distribution of composition of solid planets and the distribution in core mass of giant planets, both of which we have chosen somewhat arbitrarily, as there are very few observational constraints of the distributions of exoplanet structure and composition. But overall, we note that details such as this will not affect the overall normalization of the FPP curve (that is dictated by the assumed planet occurrence rate and the calculated priors for the false positives), just its particular shape as a function of  $\delta$ .

We emphasize that in this analysis the only information about the transit that we have considered is the



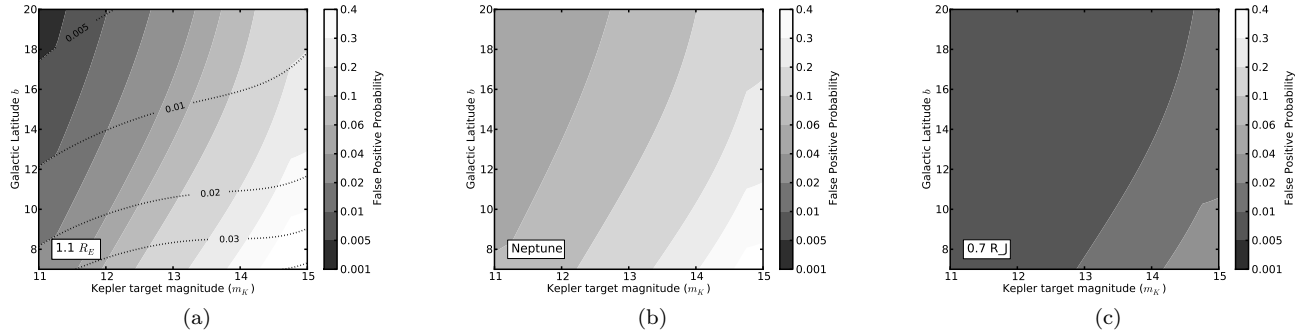


FIG. 8.— These plots illustrate the behavior of *Kepler* false positive probability (FPP) as a function of target star magnitude ( $m_K$ ) and Galactic latitude  $b$ , for three particular choices of transit depth  $\delta$ , all plotted with the same color scale. A planet occurrence rate of 20% is assumed. These plots are similar to Figure 3 except for they take into account both the changing blend radius as a function of  $m_K$  and  $\delta$  (Equation 18) and the relative likelihoods of false positives and planets at the chosen values of  $\delta$ . These particular values of  $\delta$  ( $1.1R_{\oplus}$ ,  $R_{\text{Nep}}$ , and  $0.7R_J$ ) are chosen to highlight features of how FPP changes with  $\delta$  (Figure 7). It is perhaps surprising to note that over much of this space a Neptune-sized signal has higher FPP than an Earth-sized signal; this is both because the  $\delta$  distribution for physical triple false positives peaks around  $\delta$  corresponding to a Neptune radius and because our theoretical radius distribution predicts relatively few Neptune-sized planets (Figure 5). The dotted lines in panel (a) show the FPP contours if the blend radius were restricted to  $2''$ , illustrating the power of a single deep high-resolution observation.

depth. Certainly more information can and should be used in the detailed analysis of any individual system. For example, one might include period dependence in the likelihood function by comparing the period distribution of known binary and triple systems to an assumed period distribution of planets, the way we have done with  $\delta$ . While we do not present the results of such an analysis, we have explored it and find that it decreases the derived FPP, as binary systems tend to be of longer period than planets, as far as current data can indicate. Thus, not including this analysis allows us to avoid making unwarranted assumptions about the period distribution of exoplanets while remaining consistent with our philosophical approach; that is to determine a conservative upper limit to the FPP.

Similarly, one might incorporate the additional information available from the transit light curve shape, such as the ingress/egress and transit durations, enabling a determination of the density of the eclipsed star, and thus ruling out background eclipsed giants (Seager & Mallén-Ornelas 2003). Such analysis of individual light curves is certainly desirable, and is likely already a part of the *Kepler* pipeline; however we choose not to include this additional vetting into our false positive rate analysis. Again, this choice is consistent with our overall approach, as it preserves simplicity and could cause us only to overestimate FPP.

A promising application of this FPP framework is to use the distribution of *Kepler* candidates to constrain the shape of the true mass distribution of close-in planets. Each candidate can be assigned a preliminary FPP

based on an initial assumption of the mass function, and then the observed distribution of radii can be compared to the distribution predicted from that mass function, suggesting changes to the initial assumption, and the process iterated until convergence. We plan to apply this procedure to the full *Kepler* sample of candidates.

This work also provides guidance for *Kepler* follow-up efforts. We find that the radius of possible blends is the largest single factor that can significantly raise the FPP, especially for shallower transits, and thus that deep high-resolution and high-contrast AO imaging will be key to becoming more secure about the nature of Earth-like transit signals. On the other hand, intermediate-depth candidates, corresponding to planets around the size of Neptune, will benefit most from deep high-resolution optical or IR spectroscopy, in order to constrain hierarchical triple systems, which give the largest contribution to the FPP at those depths. And of course all of these efforts will assist and be assisted by the more detailed light curve modeling of Torres et al. (2011), which will be able to determine more precise FPPs for individual systems.

We gratefully acknowledge Ed Turner and Scott Gaudi for their thoughtful and detailed comments on earlier drafts of this paper. We also thank Geoff Marcy, Steve Bryson, and Guillermo Torres for their useful discussions related to the *Kepler* mission at the January 2011 AAS meeting. We thank Jessica Lu for bringing TRILEGAL to our attention. Finally, we acknowledge the dedication and hard work of the *Kepler* team for opening up this amazing new frontier in exoplanetary science.

## REFERENCES

- Almenara, J. M., et al. 2009, *A&A*, 506, 337  
 Baglin, A. 2003, *Advances in Space Research*, 31, 345  
 Basri, G., et al. 2010, *ApJ*, 713, L155  
 Batalha, N. M., et al. 2010a, *ApJ*, 713, L103  
 —. 2010b, *ApJ*, 713, L109  
 Beatty, T. G., & Gaudi, B. S. 2008, *ApJ*, 686, 1302  
 Borucki, W., et al. 2008, in *IAU Symposium*, Vol. 249, IAU Symposium, ed. Y.-S. Sun, S. Ferraz-Mello, & J.-L. Zhou, 17–24  
 Brown, T. M. 2003, *ApJ*, 593, L125  
 Chabrier, G. 2001, *ApJ*, 554, 1274  
 Chabrier, G., Baraffe, I., Allard, F., & Hauschildt, P. 2000, *ApJ*, 542, 464  
 Cumming, A., Butler, R. P., Marcy, G. W., Vogt, S. S., Wright, J. T., & Fischer, D. A. 2008, *PASP*, 120, 531  
 Evans, T. M., & Sackett, P. D. 2010, *ApJ*, 712, 38  
 Fortney, J. J., Marley, M. S., & Barnes, J. W. 2007, *ApJ*, 659, 1661  
 Gaudi, B. S. 2005, *ApJ*, 628, L73

- Girardi, L., Bertelli, G., Bressan, A., Chiosi, C., Groenewegen, M. A. T., Marigo, P., Salasnich, B., & Weiss, A. 2002, *A&A*, 391, 195
- Girardi, L., Groenewegen, M. A. T., Hatziminaoglou, E., & da Costa, L. 2005, *A&A*, 436, 895
- Hartman, J. D., Bakos, G., Stanek, K. Z., & Noyes, R. W. 2004, *AJ*, 128, 1761
- Ho, S., & Turner, E. L. 2010, *ArXiv e-prints*
- Howard, A. W., et al. 2010, *Science*, 330, 653
- Ida, S., & Lin, D. N. C. 2004, *ApJ*, 604, 388
- Jenkins, J. M., et al. 2010a, *ApJ*, 724, 1108
- . 2010b, *ApJ*, 713, L120
- Koch, D. G., Borucki, W., Webster, L., Dunham, E., Jenkins, J., Marriott, J., & Reitsema, H. J. 1998, in *Presented at the Society of Photo-Optical Instrumentation Engineers (SPIE) Conference*, Vol. 3356, Society of Photo-Optical Instrumentation Engineers (SPIE) Conference Series, ed. P. Y. Bely & J. B. Breckinridge, 599–607
- Konacki, M., Torres, G., Sasselov, D. D., & Jha, S. 2003, *ApJ*, 597, 1076
- Latham, D. W., Brown, T. M., Monet, D. G., Everett, M., Esquerdo, G. A., & Hergenrother, C. W. 2005, in *Bulletin of the American Astronomical Society*, Vol. 37, Bulletin of the American Astronomical Society, 1340–+
- Latham, D. W., et al. 2009, *ApJ*, 704, 1107
- Mordasini, C., Alibert, Y., & Benz, W. 2009, *A&A*, 501, 1139
- O'Donovan, F. T., et al. 2006, *ApJ*, 644, 1237
- Poleski, R., McCullough, P. R., Valenti, J. A., Burke, C. J., Machalek, P., & Janes, K. 2010, *ApJS*, 189, 134
- Raghavan, D., et al. 2010, *ApJS*, 190, 1
- Seager, S., Kuchner, M., Hier-Majumder, C. A., & Militzer, B. 2007, *ApJ*, 669, 1279
- Seager, S., & Mallén-Ornelas, G. 2003, *ApJ*, 585, 1038
- Tabachnik, S., & Tremaine, S. 2002, *MNRAS*, 335, 151
- Torres, G., Konacki, M., Sasselov, D. D., & Jha, S. 2004, *ApJ*, 614, 979
- Torres, G., et al. 2011, *ApJ*, 727, 24